Available online at www.sciencedirect.com

ScienceDirect

journal homepage: www.elsevier.com/locate/he

Investigation on niobium oxide coatings for protecting and enhancing the performance of Ni cathode in the MCFC

A. Meléndez-Ceballos [a,*], S.M. Fernández-Valverde [b,**], V. Albin [a], V. Lair [a], J.Á. Chávez-Carvayar [c], A. Ringuedé [a], M. Cassir [a]

[a] Chimie ParisTech, PSL Research University, CNRS, Institut de Recherche de Chimie Paris (IRCP), F-75005, Paris, France

[b] Depto. de Química, Instituto Nacional de Investigaciones Nucleares, A.P.18-1027, México D.F., C.P.11801, México

[c] Instituto de Investigaciones en Materiales, UNAM, Circuito Exterior s/n. Ciudad Universitaria, C. P. 04510, México, D. F., México

ARTICLE INFO

Article history:
Received 9 January 2016
Received in revised form
21 March 2016
Accepted 7 April 2016
Available online 10 May 2016

Keywords:
Molten carbonate
Cathode protection
Atomic layer deposition
Niobium oxide

ABSTRACT

This study addresses the problem of the nickel cathode dissolution, decreasing the lifetime of molten carbonate fuel cells, by a protective coating of Nb_2O_5 processed by atomic layer deposition ALD onto the porous cathode substrate. Samples of different thicknesses were tested electrochemically in molten Li_2CO_3-K_2CO_3 eutectic at 650 °C during 230 h by means of chronopotentiometry and electrochemical impedance spectroscopy. A significant decrease in the stabilization time with respect to the oxygen reduction potential is observed with niobium coatings, which could indicate an electrocatalytic process favoured by the presence of Nb. The structure and morphology of the coated samples are characterised by XRD, SEM and XPS before and after the electrochemical tests. Mixed lithiated Ni and Nb oxides are likely to be formed at the cathode surface. Interestingly, this Nb-containing mixed oxide not only can protect Ni cathode but also maintains its good performance.

Introduction

There are several types of fuel cells available commercially, each one aims at satisfying a specific niche of clean generated power, portable, mobile or stationary. Molten carbonate fuel cells (MCFC) are better suited for large-scale stationary generation of several MW, more than any type of fuel cell in the market. MCFC device does not use any precious metal as catalyst making it cheaper to manufacture. Hence, MCFC is an interesting technology for producing clean energy from hydrocarbons, biogas or hydrogen-rich fuels.

The most common material used as MCFC cathode material is nickel, which undergoes *in situ* oxidation and lithiation in the carbonate melt, then nickel starts dissolving and, after reacting with hydrogen, might precipitate as

* Corresponding author.
** Corresponding author.
E-mail addresses: arturo.melendez@chimie-paristech.fr (A. Meléndez-Ceballos), suilma.fernandez@inin.gob.mx (S.M. Fernández-Valverde).

http://dx.doi.org/10.1016/j.ijhydene.2016.04.045

metallic nickel onto the anode, causing a short-circuit between both electrodes through the electrolyte [1,2]. One of the best solutions is to deposit a protective coating of a selected metal oxide onto the cathode. There are many studies dedicated to this approach in the literature, sol–gel, electrochemical deposition, chemical vapour deposition, plasma and laser sputtering of various metal oxides. For instance, CeO_2, TiO_2, Co_3O_4, Fe_2O_3, and mixtures of those have been studied with some significant results [3–10]. Nevertheless, even though addition of such layers decreases Ni solubility, they may also increase the cathode resistance and drop the cathode electrochemical performance. In recent studies, we have used atomic layer deposition (ALD), technique which allows processing ultra-thin and conformal layers, *e.g.* CeO_2, TiO_2, Co_3O_4, in order to maintain the electrocatalytic properties of the porous nickel substrate [11–13]. Interesting results were obtained, but there is still a need of more performing coatings, combining a protective role and electrocatalytic properties. Niobium compounds and, in particular oxides, are well known for their catalytic properties for oxidation processes; for instance, E. Heracleus et al. and A. Qiao et al. have used Ni-Nb-O and Ni-Nb-M-O compounds for catalysing the oxidative dehydrogenation of ethane reaction, explaining the increased activity of the Ni-O catalyst by the increased surface acidity conferred by Nb species at the surface [14–16]. Nevertheless, other authors have analysed the properties of niobium oxides for reduction processes. A. Takagaki et al. and R. Ohnishi et al. evaluated the performance of niobium oxides as catalysts for oxygen reduction reaction (ORR) in proton exchange membrane fuel cells (PEMFC) with good results [17,18]. As far as we know there are no specific mechanistic studies on niobium oxides grown on nickel oxide substrates [19,20]; however, pre-oxidised nickel-niobium alloy has already been suggested by Fang et al. as novel candidate material for replacing the classical nickel oxide cathode [21,22]. These authors obtained a significant drop in Ni solubility (8 10^{-6} instead of 17 10^{-6} mol fraction). They also mentioned that niobium oxide cannot be thermodynamically reduced by H_2 or CO in the anode MCFC atmosphere, which is favourable to the application because no metallic niobium would be deposited in the electrolyte.

In the present study, we investigated for the first time the structural, morphological and electrochemical behaviour of ALD-processed thin layers of different thicknesses of Nb_2O_5 onto the commercial porous Ni cathode. ALD is a chemical gas phase deposition technique first developed in Finland in the 1970s by T. Suntola et al. [23,24]. In ALD, reactant gas pulses are introduced separately in order to reach the substrates to be coated and growth is achieved through self-terminating surface reactions, which means that only one monolayer of reactant gas species can be adsorbed to the surface during a pulse. We worked in Li_2CO_3-K_2CO_3 bulk at 650 °C in conditions simulating MCFC cathode operation. Our aim here is to show whether ALD-processed niobium oxide coatings could play a protective role with respect to Ni cathode and maintain or improve the electrocatalytic properties of nickel. A deeper insight contemplating the mechanistic effect of niobium with respect to oxygen reduction kinetics is out of the scope.

Experimental

Atomic layer deposition of Nb_2O_5

A thin layer of Nb_2O_5 was deposited on a commercial porous nickel substrate (produced by Doosan Company, South-Korea) by means of ALD technique using a vertical flow type reactor (Picosun SUNALE™ R-series). Niobium ethoxide, $Nb(OCH_2CH_3)_5$ (Sigma–Aldrich®) was used as precursor and distilled water as oxidizing agent. In order to process the Nb_2O_5 layer, $Nb(OCH_2CH_3)_5$ was introduced into the precursor chamber using the following conditions: precursor pulse time 0.5 s, purge time 3 s, N_2 line flow of 100 cm^3 min^{-1}, water pulse time 0.1 s purge time 3 s [25]. The precursor was sublimated at 80 °C and the water vapour was supplied at 25 °C. The reactor temperature was kept at 300 °C with a N_2 flow of 300 cm^3 min^{-1}, the precursor pulse and purge was followed by water pulse and purge, this cycle was repeated until the desired thickness was reached. The growth rate of Nb_2O_5 layers over the porous nickel substrate was ≈1 Å/cycle. Four different samples were processed by this technique to obtain 5, 20, 50 and 300 nm deposited layers.

Material characterization

Deposited layers were characterized by X-ray diffraction, SEM and XPS. XRD was performed in a PANalyticalX'pert Pro from Anton Paar with Cu–$K_\alpha 1$ radiation (λ = 1.54056 Å). The diffraction pattern was obtained by scanning between 20 and 120° by steps of 0.02 (2θ°) with a fixed counting time of 2.3 s in razing mode. Once the data were obtained, Scanning Electron Microscopy (SEM) analysis were performed with a ZEISS® Ultra 55 microscope to evaluate the surface, morphology and to measure the layer thickness. X-ray photoelectron spectra were recorded using a Thermo Scientific K-Alpha X-ray photoelectron spectrometer with a monochromator Al Kα X-ray (hν = 1486.61 eV) for sample excitation. An argon ion beam was used to prevent sample surface charging. The spectrometer energy calibration was obtained using Au 4f 7/2 and Cu 2p 3/2 photoelectron lines. The position of the adventitious carbon C 1 s peak at 284.6 eV was used as an internal reference in each sample to determine the binding energies with an accuracy of ±0.1 eV. The residual pressure in the analysis chamber was maintained below 10^{-8} Torr, during data acquisition. Three samples of 50 nm niobium oxides deposited on porous nickel were analysed, one as-deposited and two others M1 and M2 after immersion in molten carbonate eutectic at 650 °C for 44 h and 144 h respectively. The survey spectrums were obtained between 0 and 1000 eV, for all samples. The spectra were collected and analysed with Advantage 4.0 software.

Electrochemical cell

Lithium and potassium carbonates, of high-grade purity >98% (Sigma–Aldrich®), were mixed in a proportion of 62:38 mol %. The high-temperature electrochemical cell was a single-compartment crucible of dimensions 70 × 50 mm^2 contained in an alumina Al_2O_3 reactor of dimensions 250 × 60 mm^2

hermetically sealed by a stainless steel cover with a Viton O-ring. The whole electrochemical set-up was fully described in a previous papers [26]. Temperature was controlled at a constant value of 650 °C by means of a calibrated chromel/alumel thermocouple. The standard cathode atmosphere was a mixture of O_2/CO_2/Ar (14:30:56 atm. %) of high-grade purity (Air Liquide®) at 650 °C and a pressure of 1 atm. After stabilizing the molten carbonate eutectic under the selected cathode atmosphere, each sample was immersed in the molten carbonate eutectic and was used as working electrode to perform electrochemical measurements.

Electrochemical measurements

The electrochemical experimental data were collected using a potentiostat/galvanostat (AutoLab® PGSTAT-302N with FRA module). A three-electrode system was used, the working electrode being the modified porous Ni cathode ($10 \times 10 \times 0.5$ mm), the counter electrode was a gold wire and the reference electrode a silver wire dipped into an Ag_2SO_4 (10^{-1} mol kg^{-1}) saturated electrolyte eutectic melt into an alumina tube sealed by a porous alumina membrane. Open circuit potential (OCP) was measured for a period of 230 h for the modified cathodes. The parameters used for impedance (EIS) measurements are the following: scanning frequencies set from 10^{-3}–10^{6} Hz, with 11 points per decade, and signal amplitude of 5 mV respecting the system linearity. The fitting of the equivalent circuit was performed with Zview® V3.3e software.

Ni solubility

The solubility of bare porous nickel and 20 nm Nb_2O_5 coated porous nickel was measured individually from the different $(Li_{62}\text{-}K_{38})_2CO_3$ melts used in the experiments. Small amounts of carbonates (about 1.4 g) were withdrawn randomly three times from the molten carbonate bulk at the end of the electrochemical characterizations, which corresponds to 230 h immersion. After solidification, each carbonate sample was hand-milled to obtain a fine powder. 2 g of carbonate powder were then dissolved in 10 ml of HNO_3 at 3 vol %. Nickel content was determined by ICP-AES (ICAP 6000 Series from Thermo Fisher Scientific). The calibration was performed using Aldrich atomic absorption standard solutions, dissolved in HNO_3 at 3 vol. %.

Results and discussion

Material characterization

In Fig. 1, a comparison of SEM micrographs of the as-deposited Nb_2O_5 with thicknesses of 300 (a), 50 (b) and 5 (c) nm are shown. As can be observed, ALD deposits are dense, conformal and homogenous as expected. It should be noted, however, that the thinner is the layer the more it seems fragile, which is specifically the case in Fig. 1b) for a 5 nm coating. X-ray diffraction pattern shown in Fig. 2 was obtained from a sample coated with 300 nm of Nb_2O_5 over Si (0 0 1) and heat treated at 650 °C for 4 h. Further analysis by software indicates the presence of 3 phases corresponding to ICDD pattern numbers 00-030-0873, 00-026-0885 and 01-071-0020 that belong to an orthorhombic Nb_2O_5, monoclinic Nb_2O_5 and tetragonal NbO_2 type crystals, respectively. Orthorhombic Nb_2O_5 constitutes the primary phase. The peak located at 2θ° value of 99.5211 was not identified as part of the previously mentioned phases. The average crystal size deduced from the peaks after applying the Sherrer equation is around 65 nm [27]. The different phases and consequent Ni and Nb valences, as well as lattice defects present in the material could facilitate the interaction of Nb with the undelaying Ni and possibly accelerate Li penetration which could play a favourable role in the cathode electrochemical behaviour.

XPS spectra of Nb (a), Ni (b) and O (c) peaks for the as-deposited 50 nm Nb_2O_5 coated nickel (1), samples after 44 h (2) and 144 h (3) immersion in the carbonate melt are shown in Fig. 3. The values of peak position and peak area in percentage as well as the related phases are summarized in Table 1. For each binding energy determination, the values obtained were corrected with respect to adventitious carbon taken as reference. In Fig. 3, changes in binding energies and percentages of different niobium, oxygen and nickel species are observed. In Fig. 3a_1, Nb $3d_{5/2}$ and Nb $3d_{3/2}$ are found at 207.5 eV and 210.2 eV, respectively, and correspond to Nb_2O_5 [28]. The Ni XPS spectrum in Fig. 3b_1 shows four peaks, the first peak at 852.5 corresponds to $2p_{3/2}$ Ni [29], probably present at the surface due to sample handling. Peaks at 855 and 860.3 eV belong to $2p_{3/2}$ and $2p_{3/2}$ satellites of NiO, respectively [30–32] the peak at 857 eV could be due to the presence of Ni-OH bonds as suggested by the literature [33,34]. The O spectra in Fig. 3c_1 shows the presence of two 1 s peaks, one at 530.5 eV which corresponds to the oxygen contained in Nb_2O_5 and NiO [31,35,36]. The peak present at 532.2 eV corresponds to O-H bonds found in molecular chemisorbed water or hydroxyl surface groups [31,33,37] maybe present due to sample handling. After 44 h in the carbonate melt, sample M1 (see Fig. 3a_2) shows clearly a change in shape and two new peaks appear on the spectra. Peaks at binding energies of 206.5 eV and 209.1 eV should correspond to a Li-Nb-O phase with defects or oxygen vacancies hence a lower binding energy than the values reported for $LiNbO_3$ [38,39]. Diffusion of Nb into Ni could have lower the binding energy of Nb_2O_5 peaks at 209.9 and 207.4 eV by replacing some Nb-O ligands by Ni-Nb this shift on Nb for Ni-Nb-O phases has been reported in literature [36,40]. In the case of Ni, the peak at 852.5 eV disappears. The $2p_{3/2}$ NiO peak, originally at 855 eV, is split in two peaks, one at 854.5 eV and another at 856.5 eV corresponding, most probably, to Ni^{II} and Ni-O defects, respectively [37,41]. The satellite $2p_{3/2}$ is displaced to a higher BE value of 861.2 eV. The observed shifts are proper to Li incorporation into the NiO matrix [41] and also could be due to Nb incorporation to form a more complex Li-Ni-Nb-O phase. A peak appearing at 865.5 eV could evidence the formation of a Nb_2O_5-rich NiO compound, such as $NiNb_2O_6$ similar to $NiFe_2O_4$ which presents also a peak at that BE [34]. Oxygen peak also shows a split in two contributions, one at 529.4 eV attributed to O 1 s of Li-Ni-O bonds [41] and another at 530.8 eV from the Nb-O bonds [39]. In sample M2, the binding energy of Nb $3d_{3/2}$ remain as in M1, while the

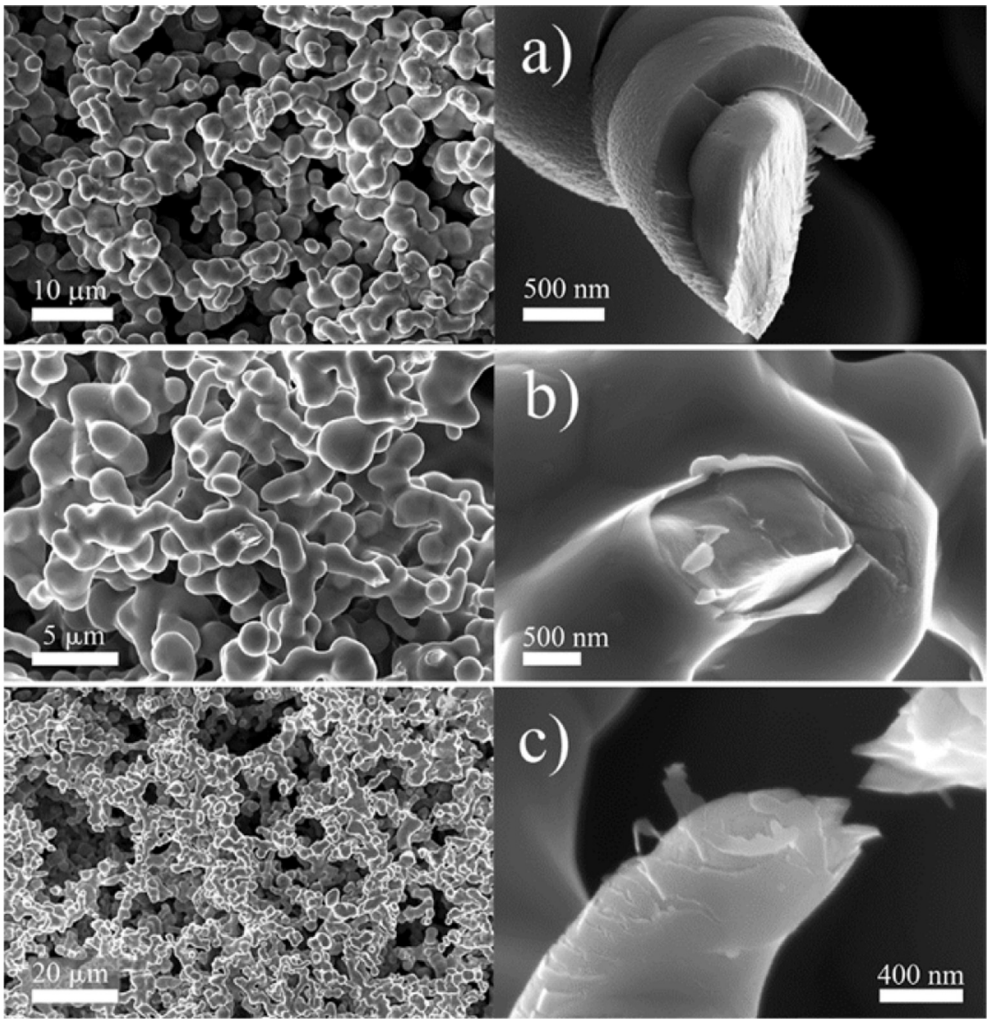

Fig. 1 – SEM images of the as-deposited Nb_2O_5 thin layers. Left side low magnification, right side high magnification close to a broken Ni grain. Thicknesses are: a) 300 nm, b) 50 nm, c) 5 nm layers.

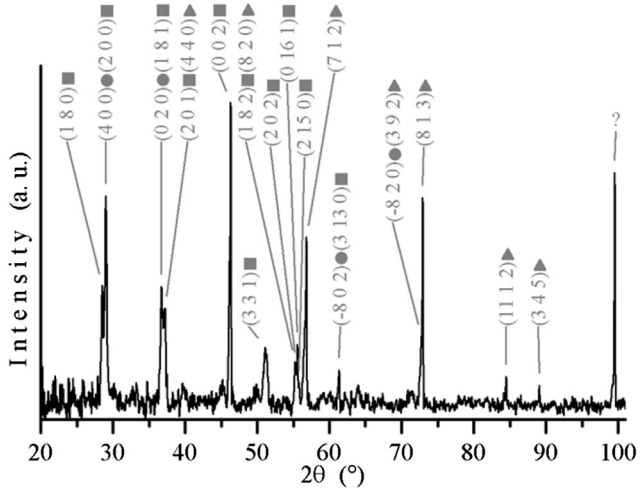

Fig. 2 – X-ray diffractogram of 300 nm Nb_2O_5 layer showing three identified phases: (■) Orthorhombic Nb_2O_5 ICDD (00-030-0873), (●) Monoclinic Nb_2O_5 ICDD (00-026-0885) and (▲) Tetragonal NbO_2 ICDD (01-071-0020). ? = unidentified peak at 99.5211 (2 θ°). In parenthesis the (h k l) numbers of the corresponding phase.

$3d_{5/2}$ peak is shifted to a BE of 207.1 eV; this shift has been reported by Trifonov et al. in the oxidation of Ni-Nb alloys [40]. In our case, it might reflect further Nb an Li intercalation into the subjacent NiO, forming a Li-Ni-Nb-O phase. The Nb peaks at BE 209.4 and 206.5 eV correspond to the BE energies of $LiNbO_3$, as shown by Aufray et al. [38]. Nb_2O_5 being available at the surface of the electrode, it is not surprising that lithiation of Nb_2O_5 takes place. In the case of Ni $2p_{3/2}$, peaks are shifted again to a lower BE of 854.3 and 856.1 eV, as previously mentioned they correspond to Ni^{II} and Ni-O defects, respectively. As can be noticed in Table 1, the area of the peaks has also changed and an increase from 25 to 33% in the peak area for the Ni-O defects might be caused by further Li and Nb incorporation in to the NiO lattice. Ni $2p_{3/2}$ satellite increased its BE to 861.3 eV and the peak at 865 remains. All Ni peaks indicate a strong Li and Nb interaction with NiO forming a Li-Ni-Nb-O pase [41,42]. Oxygen peaks show an increase in BE in respect to M1 sample and are now at 531.3 and 529.7 eV. According to Pawlak et al. [43] oxygen 1 s spectra, is affected by the different metals present on the coordination shell of oxygen; thus, the shift in O1 s peaks could be due to the presence

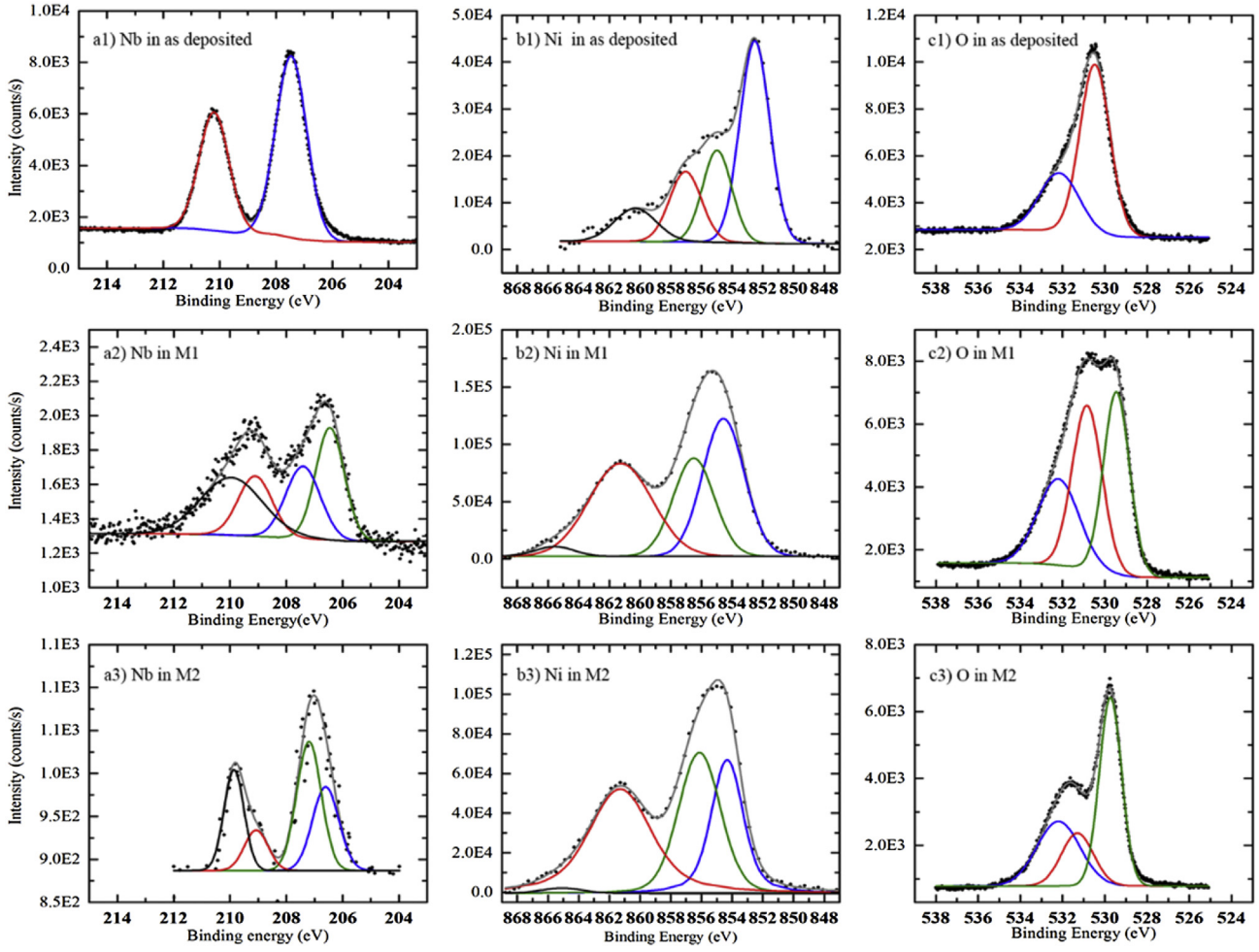

Fig. 3 – XPS spectra of all tested samples, a1), b1) and c1) corresponding to Nb_2O_5 as deposited on porous nickel by ALD, a2), b2) and c2) corresponding to sample M1 obtained after 44 h immersion time in a mixture of Li and K carbonates at 650 °C and a3), b3) and c3) corresponding to sample M2 obtained after 144 h of immersion in the same conditions.

of Li-Ni-Nb-O phase. It is clear that the complex interaction between NiO, Nb_2O_5 and Li^+ in our media will require a more detailed XPS study to determine unambiguously the precise composition of the cathode surface after a long immersion in the molten $(Li_{62}\text{-}K_{38})_2CO_3$ eutectic.

Electrochemical characterization

Fig. 4 shows the evolution of the open circuit potential (OCP) for each tested sample over 230 h, corresponding to porous nickel and Nb_2O_5 coatings of 5 nm, 20 nm, 50 nm and 300 nm, respectively. As can be noted in Fig. 4, porous Ni follows a 2 step potential evolution where the plateaus are denoted as I (≈−0.68 V), II (≈−0.37 V) and III (≈0 V). The OCP behaviour of porous nickel has been investigated by different authors, among them Yazici et al. and Antolini [44,45], who attributed the steps to the *in situ* Ni oxidation followed by the NiO lithiation process on the porous nickel surface. The three plateaus corresponding to porous nickel, observed in Fig. 4, are related to the modification of the porous Ni electrode into $Li_xNi_{1-x}O$, in a progressive way. The first plateau (I) from 0 to 98 h is ascribed to the *in situ* oxidation of metallic nickel, after the first potential jump at 98 h, a second plateau (II) is reached at a potential around −0.4 V/(Ag/Ag^+). This plateau corresponds to the *in situ* lithiation of NiO, which is probably associated to an increase in the nickel valence from Ni^{2+} to Ni^{3+}, as reported by Nishina et al. from XPS measurements [46]. At equilibrium, lithium content in NiO cathode was estimated by nuclear microprobe to be roughly 0.2 at% [47]. After 182 h, the lithiation process is completed and the third plateau (III) at −0.03 V/(Ag/Ag^+) corresponds to an equilibrium potential between O_2, CO_2 and carbonates. At this stage, the electrode works as a stable cathode for oxygen reduction.

Samples coated by a thin layer of Nb_2O_5 do not show the same behaviour as bare porous nickel. The 300 nm coated sample, shown in Fig. 4, reaches a potential around −0.4 V/(Ag/Ag^+) very fast, in less than 25 h, and appears relatively stable until 63 h. Then, it increases slowly (in absolute value) with a mild slope until reaching −0.45 V/(Ag/Ag^+) and remains relatively stable. Apparently, this Nb_2O_5 layer is too thick and blocks the nickel catalytic activity. When decreasing the thickness of the layer to 50 nm, as shown in Fig. 4, the OCP behaviour seems more favourable; even though it does not follow completely the Ni behaviour, it shows two potential

Table 1 – Peak data obtained from XPS spectra fitting shown in Fig. 3. Peak numbers are designed from high to low binding energies.

	Nb peaks				Ni peaks				O peaks			
	Peak number	Center (eV)	Area (%)		Peak number	Center (eV)	Area (%)		Peak number	Center (eV)	Area (%)	
As deposited	1	210.2	39	$3d_{3/2}$ Nb_2O_5	1	860.3	11	$2p_{3/2}$, sat NiO	1	532.2	31	1s H_2O
	2	207.5	61	$3d_{5/2}$ Nb_2O_5	2	857	18	Ni-OH	2	530.5	69	1s Nb_2O_5/NiO
					3	855	22	$2p_{3/2}$ NiO				
					4	852.5	49	$2p_{3/2}$ Ni				
As in M1	1	209.9	31	$3d_{3/2}$ Nb_2O_5	1	865.5	2	$NiNb_2O_6$?	1	532.2	27	1s H_2O
	2	209.1	18	$3d_{3/2}$ $LiNbO_3$	2	861.2	37	$2p_{3/2}$, sat Li-Ni-Nb-O	2	530.8	37	1s Nb-O
	3	207.4	22	$3d_{5/2}$ Li-Ni-Nb-O	3	856.5	25	$2p_{3/2}$ Li-Ni-Nb-O	3	529.4	36	1s Li-Ni-O
	4	206.5	28	$3d_{5/2}$ $LiNbO_3$	4	854.5	36					
As in M2	1	209.9	15	$3d_{3/2}$ Nb_2O_5	1	865	2	$NiNb_2O_6$?	1	532.2	29	1s H_2O
	2	209.4	20	$3d_{3/2}$ $LiNbO_3$	2	861.3	39	$2p_{3/2}$, sat Li-Ni-Nb-O	2	531.3	23	1s Li-Nb-O
	3	207.1	48	$3d_{5/2}$ Li-Ni-Nb-O	3	856.1	33	$2p_{3/2}$ Li-Ni-Nb-O	3	529.7	51	1s Li-Ni-Nb-O
	4	206.5	18	$3d_{5/2}$ $LiNbO_3$	4	854.3	26					

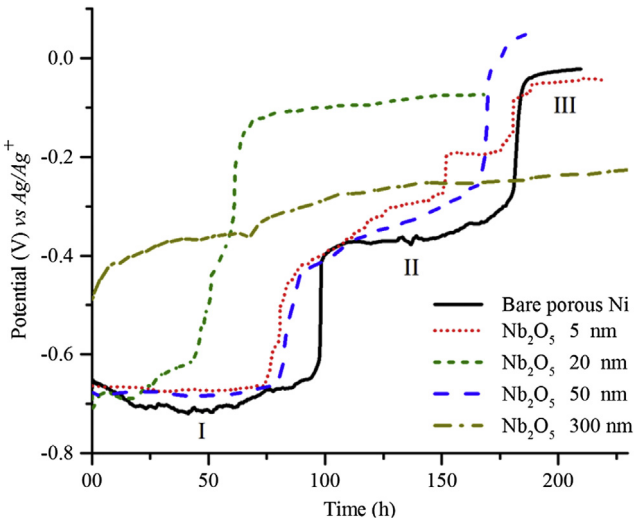

Fig. 4 – Opencircuit potential evolution *vs.* time over 230 h for porous Ni and Nb_2O_5 covered samples immersed in molten Li_2CO_3-K_2CO_3 eutectic at 650 °C.

steps. The first one occurs at 81 h, before that of nickel, up to a potential of −0.42 V/(Ag/Ag$^+$) and continues increasing with a slight slope until 166 h where it jumps from −0.25 to −0.02 V/(Ag/Ag$^+$) at 171 h, to finally reach its maximum potential 0.05 V/(Ag/Ag$^+$) at 187 h. This behaviour indicates that nickel oxide is acting as a catalyst and the presence of Nb_2O_5 somehow accelerates the potential evolution reaching a favourable working potential in a shorter time. If we reduce the thickness of the protective Nb_2O_5 layer to 20 nm, as depicted in Fig. 4, the behaviour changes drastically from that of porous Ni and the 50 nm coated sample, showing a very small potential increment after 24 h immersion from −0.66 to −0.60 V/(Ag/Ag$^+$) at 44 h. Then the potential increases rapidly from −0.60 to −0.1 V/(Ag/Ag$^+$) at 79 h. Afterwards, the potential increases slowly during the next 89 h of the experiment, reaching a final value of −0.07 V/(Ag/Ag$^+$) after 168 h of immersion in the molten carbonate melt at 650 °C. For the 20 nm coated sample, shown in Fig. 4, a good working potential is reached 112 h before the porous Ni electrode, which could indicate that the presence of Nb_2O_5 is increasing the catalytic properties of NiO or even that Nb_2O_5 is acting as a catalyst itself. It seems that the 20 nm is the most efficient coating with respect to the stabilisation of the Ni electrode.

The 5 nm Nb_2O_5-coated sample, described in Fig. 4 shows a behaviour close to that of the 50 nm coated sample and porous Ni. The initial potential remains stable at around −0.66 V/(Ag/Ag$^+$) during 74 h when it starts to rise up to −0.42 V/(Ag/Ag$^+$). Then if follows a slope similar to the 50 nm sample up to −0.27 V/(Ag/Ag$^+$) at 150 h when it presents a fast increase in the form of a step up to −0.18 V/(Ag/Ag$^+$) that remains stable until 175 h. After another potential step, it reaches a value of −0.05 V/(Ag/Ag$^+$) remaining stable for the rest of the experiment. It seems that the first part of the OCP behaviour corresponds to the influence of Nb_2O_5, while the final two steps are a direct influence of the Ni oxidation/lithiation phenomenon already described. This hypothesis seems to be supported by the fact that the content of Nb_2O_5 is very small and even though it influences the OCP behaviour, the final potential step occurs at the same time as the bare porous Ni reaching a potential around −0.04 V, which is a good value in terms of cathode equilibrium potential.

Even though the 20 nm and 50 nm coated samples could be considered close in term of thickness, their OCP behaviour is not. The difference is due to the fact that the 20 nm sample could be more reactive towards NiO than the 50 nm sample, forming faster a mixed valence Li-Ni-Nb-O phase, as suggested by XPS analysis, that could stabilise the cathode faster than $Li_xNi_{1-x}O$ phase and probably act as a good electrocatalyst. In the 50 nm sample, the presence of Nb_2O_5 at the extreme surface in contact with carbonates could block the effect of the mixed phase at the NiO-Nb_2O_5 interphase.

Electrochemical impedance spectroscopy data were recorded periodically and fitted to deduce resistance values, such as charge transfer resistance (R1), mass transfer resistance (R3) and total resistance (Re + R1 + R2 + R3) of the electrochemical system. Fig. 5 shows an example of data fitting and the corresponding equivalent circuit. It is necessary to consider a three-phenomenon circuit with a series of three sets of a resistor in parallel with a constant phase element (CPE) due to the presence of an arc at medium frequencies. The presence of this arc has been discussed by Escudero et al. [48], suggesting that this phenomenon, observed only during the first 8 h, is due to the formation of the $Li_xNi_{1-x}O$ phase. In our case, this phenomenon is present along the 230 h for most of the samples except the 20 nm one. It is difficult to explain this phenomenon, probably not due to the oxidation/lithiation of Ni but maybe to the porosity of the material; anyhow, it is not our purpose to analyse deeply the origin of this middle frequency arc, which would require analysing the evolution of the distribution of relaxation times (DRT).

It is worth mentioning that for comparison, resistances and EIS data are presented at a similar OCP value instead of a given time; we have opted for this representation since the samples behave differently with respect to time. Fig. 6 shows different EIS data taken along 130 h of immersion time for the 20 nm-coated sample. We can note an increase in the total resistance *vs.* time up to 65 h, which is due to the growth of the

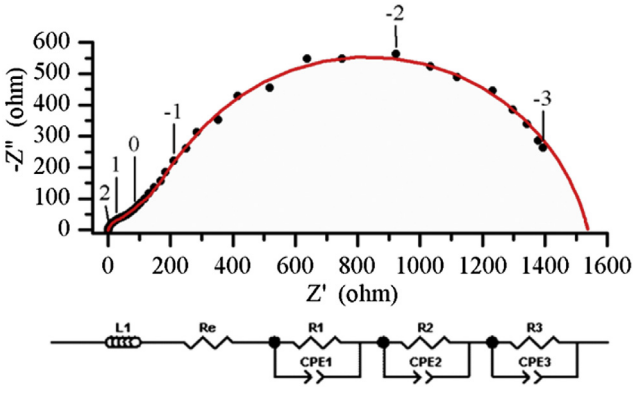

Fig. 5 – Nyquist representation of EIS data (●) of 50 nm Nb_2O_5 covered sample taken at 176 h immersion in molten Li_2CO_3-K_2CO_3 eutectic at 650 °C. Fitted with the equivalent circuit shown above (—). Numbers correspond to the logarithm of the frequency.

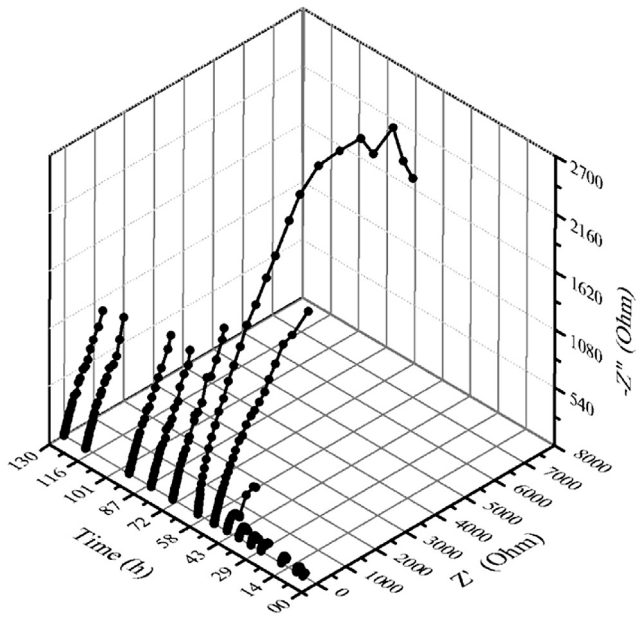

Fig. 6 – Nyquist representation of impedance data taken periodically over 130 h. Data corresponds to the 20 nm covered sample immersed in molten Li_2CO_3-K_2CO_3 eutectic at 650 °C.

Table 2 – Charge transfer resistance (Rtc) and total resistance (Rtot) for each sample tested, taken from EIS data fitting at a comparable OCP value after the last potential step and close to 0 V.

	Rtc	Rtot
Porous Ni	2.3	350
5 nm	1.2	745
20 nm	12	1200
50 nm	29	1500
300 nm	101	1950

nickel oxide layer in interaction with the Nb_2O_5 ultrathin layer. After 65 h, the total resistance decreases, which is consistent with the lithiation of NiO and/or Nb_2O_5 increasing the conductivity. Nevertheless, the total resistance deduced from the impedance data at OCP potential around −0.07 V/(Ag/Ag^+) is 4 times higher than that of bare porous Ni at similar potential. In Table 2, the influence of Nb_2O_5 layer thickness over the charge transfer resistance and total resistance is evidenced at their final steady state potential for all the samples. As could be expected due to the high resistivity of Nb_2O_5, the charge transfer resistance increases when increasing the thickness as do the total resistance. Nevertheless, resistance values shown by the 5 nm and 20 nm samples could still be acceptable for MCFC cathode application. Fig. 7 shows a comparison of the Nyquist diagrams obtained for each sample at a similar potential close to 0 V/(Ag/Ag^+). In this figure, we can observe that the 20 nm Nb_2O_5 coated sample seems to have a different diffusion regime than all the rest, probably due to a faster adsorption–desorption kinetics of dissolved oxygen and CO_2 at the surface of the electrode.

Fig. 8 shows the evolution of the total resistance (Rtot) for all the samples over immersion time. All the Nb_2O_5 coated samples present an increase in resistance up to a maximum that occurs before the final potential step: 169 h for 5 nm, 61 h for 20 nm and 163 h for 50 nm. This is not true for the porous Ni sample, which presents its maximum resistance at 189 h, just after the potential step. After reaching the maximum resistance value, all the samples show a significant resistance decrease due most likely to the formation of $Li_xNi_{1-x}O$ or a mixed Li-Ni-Nb-O phase, more conductive than NiO. It is important to notice that the 20 nm sample shows a promising OCP behaviour knowing that the solubility of Ni decreases and that a catalytic effect of Nb is likely. It is important to point out two key points on the electrochemical study performed. The first is that the OCP of 20 nm coated Ni reaches rapidly a potential around 0 V/(Ag/Ag^+) due to a rapid oxidation and lithiation of Ni; the second is that total resistance increases up to 8633 Ω and then decreases to a minimum value of 1200 Ω. Even though the final resistance is high, this resistance drop cannot

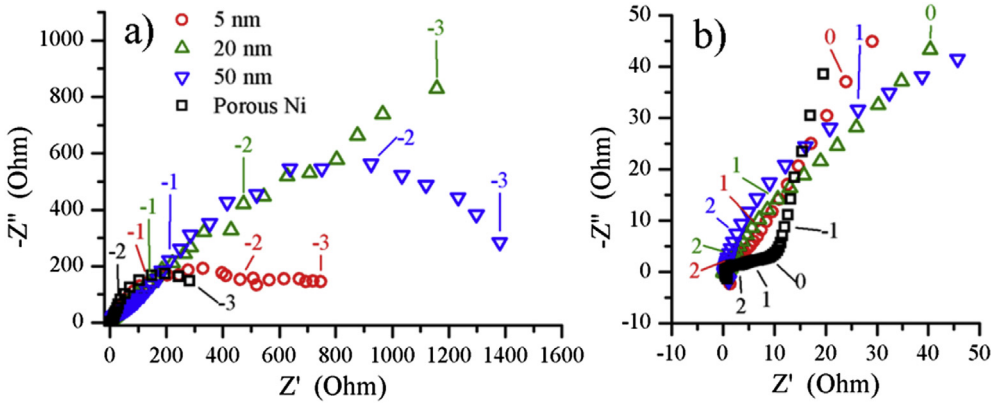

Fig. 7 – Superposed Nyquist diagrams of EIS data taken at plateau III (Fig, 5). a) General over view, b) Zoom into high frequency area. OCP voltage was around 0 V. All data taken with samples immersed in molten Li_2CO_3-K_2CO_3 eutectic at 650 °C. Samples were: bare porous nickel (■), 5 nm (●), 20 nm (▲) and 50 nm (▼) covered samples. Numbers correspond to the logarithm of the frequency.

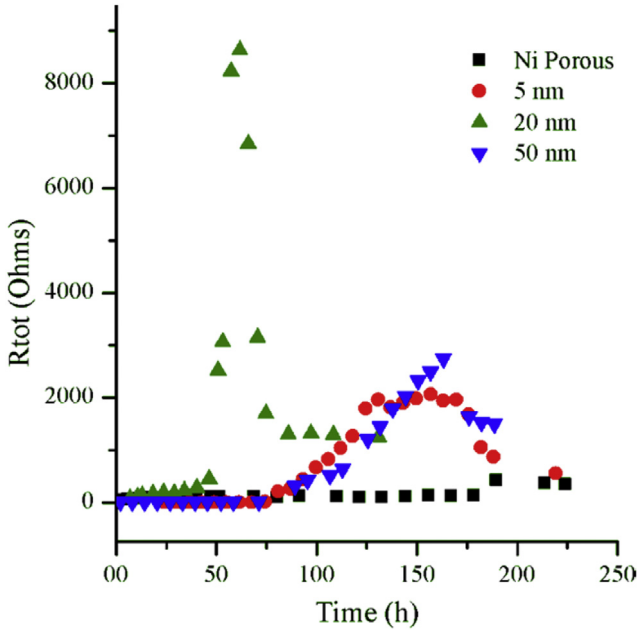

Fig. 8 – Total resistance evolution (Rtot = Re + R1 + R2 + R3) over time for: bare porous nickel (■), 5 nm (●), 20 m (▲) and 50 nm (▼) covered samples immersed in molten Li_2CO_3-K_2CO_3 eutectic at 650 °C.

be due only to lithiation, but to the presence of a mixed oxide phase. Further specific studies on the reduction kinetics of oxygen on the Nb-coated porous nickel cathode are necessary to determine whether Nb at surface is really facilitating the mass transport process of oxygen.

Solubility of Ni in molten Li-K eutectic carbonates was measured by means of ICP-AES to evaluate the protection conferred by the Nb_2O_5 coating. It can be seen that in comparison with bare porous Ni cathode with a solubility in molten Li_2CO_3-K_2CO_3 (62–38 mol %) eutectic carbonates at 650 °C of 15 wt. ppm, the 20 nm Nb_2O_5 protective layer reduced the Ni dissolution to 10 wt. ppm in strictly the same conditions. This demonstrates that coating the bare porous nickel cathode material with an ultra-thin layer of Nb_2O_5 is effective to protect the cathode of MCFC and, hence, for increasing its lifetime.

Conclusions

ALD-processed layers Nb_2O_5 were deposited onto porous nickel MCFC cathode in various thicknesses; as expected they were conformal and dense. Then, these samples were tested electrochemically in molten Li_2CO_3-K_2CO_3 (62–38 mol %) eutectic carbonates at 650 °C. Solubility of NiO was effectively decreased with a 20 nm Nb_2O_5 layer and the electrochemical performance shown by the OCP was satisfactory, especially for the 20 nm Nb_2O_5 covered sample, which allowed a very rapid potential increase. For the same sample, total resistance and mass transfer resistance showed an abrupt increment, followed by a rapid decrease, evidencing the presence of some kind of catalytic effect due to the presence of niobium. XPS analysis showed that mixed phases of Ni-Nb-Li-O are present in the surface of the electrode; these phases could be responsible for the apparent catalytic behaviour. Even though the influence of Nb could modify oxygen reduction at the surface of the electrode, a more detailed kinetic study will be necessary to explain the role of Nb in the reduction mechanism. In brief, we have shown that Nb_2O_5 can be used as protective material for the MCFC cathode when deposited as a fine conformal and dense layer; this layer decreasing nickel solubility, accelerating the stabilisation of the electrode (OCP behaviour) and not affecting the catalytic performance of the state-of-the-art electrode, because of the formation of a mixed compound with interesting electrocatalytic properties that would require more insight.

Acknowledgements

The authors wish to thank the program ECOS–(M13P01) for financial support and also CONACYT for the Ph.D. scholarship 314518, as well as the mexican hydrogen network program 2015.

REFERENCES

[1] Antolini E. The stability of molten carbonate fuel cell electrodes: a review of recent improvements. Appl Energy 2011;88:4274–93. http://dx.doi.org/10.1016/j.apenergy.2011.07.009.

[2] Kulkarni A, Giddey S. Materials issues and recent developments in molten carbonate fuel cells. J Solid State Electrochem 2012;16:3123–46. http://dx.doi.org/10.1007/s10008-012-1771-y.

[3] Baizeng F, Xinyu L, Xindong W, Shuzhen D. Surface modification of a MCFC anode by electrodeposition of niobium. J Electroanal Chem 1998;441:1–3. http://dx.doi.org/10.1016/S0022-0728(97)00203-9.

[4] Chauvaut V, Cassir M, Denos Y. Behavior of titanium species in molten Li_2CO_3–Na_2CO_3 and Li_2CO_3–K_2CO_3 under anodic and cathodic conditions. I – thermodynamic predictions at 550–750°C. Electrochim Acta 1998;43:1991–2003. http://dx.doi.org/10.1016/S0013-4686(97)10139-6.

[5] Chauvaut V, Albin V, Schneider H, Cassir M, Ardéléan H, Galtayries A. Study of cerium species in molten Li_2CO_3–Na_2CO_3 in the conditions used in molten carbonate fuel cells. Part I: thermodynamic, chemical and surface properties. J Appl Electrochem 2000;30:1405–13. http://dx.doi.org/10.1023/A:1026595117970.

[6] Belhomme C, Gourba E, Cassir M, Tessier C. Chemical and electrochemical behaviour of Ni–Ti in the cathodic conditions used in molten carbonate fuel cells. J Electroanal Chem 2001;503:69–77. http://dx.doi.org/10.1016/S0022-0728(01)00375-8.

[7] Albin V, Mendoza L, Goux A, Ringuedé A, Billard A, Briois P, et al. Morphological, structural and electrochemical analysis of sputter-deposited ceria and titania coatings for MCFC application. J Power Sources 2006;160:821–6. http://dx.doi.org/10.1016/j.jpowsour.2006.04.066.

[8] Mendoza L, Albin V, Cassir M, Galtayries A. Electrochemical deposition of Co_3O_4 thin layers in order to protect the nickel-based molten carbonate fuel cell cathode. J Electroanal Chem 2003;548:95–107. http://dx.doi.org/10.1016/S0022-0728(03)00228-6.

[9] Wijayasinghe A, Bergman B, Lagergren C. $LiFeO_2$–$LiCoO_2$–NiO materials for molten carbonate fuel cell cathodes. Part II. Fabrication and characterization of porous gas diffusion cathodes. Solid State Ion 2006;177:175–84. http://dx.doi.org/10.1016/j.ssi.2005.10.019.

[10] Wijayasinghe A, Bergman B, Lagergren C. $LiFeO_2$–$LiCoO_2$–NiO materials for molten carbonate fuel cell cathodes. Part I: powder synthesis and material characterization. Solid State Ion 2006;177:165–73. http://dx.doi.org/10.1016/j.ssi.2005.10.018.

[11] Meléndez-Ceballos A, Fernández-Valverde SM, Barrera-Díaz C, Albin V, Lair V, Ringuedé A, et al. TiO_2 protective coating processed by atomic layer deposition for the improvement of MCFC cathode. Int J Hydrog Energy 2013;38:13443–52. http://dx.doi.org/10.1016/j.ijhydene.2013.07.083.

[12] Meléndez-Ceballos A, Albin V, Fernández-Valverde SM, Ringuedé A, Cassir M. Electrochemical properties of atomic layer deposition processed CeO_2 as a protective layer for the molten carbonate fuel cell cathode. Electrochim Acta 2014;140:174–81. http://dx.doi.org/10.1016/j.electacta.2014.05.025.

[13] Meléndez-Ceballos A, Albin V, Ringuedé A, Fernández-Valverde SM, Cassir M. Electrochemical behavior of $M_{x-1}O_x$ (M = Ti, Ce and Co) ultra-thin protective layers for MCFC cathode. Int J Hydrog Energy 2014;39:12233–41. http://dx.doi.org/10.1016/j.ijhydene.2014.03.213.

[14] Heracleous E, Lemonidou AA. Ni–Nb–O mixed oxides as highly active and selective catalysts for ethene production via ethane oxidative dehydrogenation. Part I: characterization and catalytic performance. J Catal 2006;237:162–74. http://dx.doi.org/10.1016/j.jcat.2005.11.002.

[15] Heracleous E, Lemonidou AA. Ni–Nb–O mixed oxides as highly active and selective catalysts for ethene production via ethane oxidative dehydrogenation. Part II: mechanistic aspects and kinetic modeling. J Catal 2006;237:175–89. http://dx.doi.org/10.1016/j.jcat.2005.11.003.

[16] Qiao A, Kalevaru VN, Radnik J, Martin A. Oxidative dehydrogenation of ethane to ethylene over Ni–Nb–M–O catalysts: effect of promoter metal and CO_2-admixture on the performance. Catal Today 2016;264:144–51. http://dx.doi.org/10.1016/j.cattod.2015.08.043.

[17] Takagaki A, Takahashi Y, Yin F, Takanabe K, Kubota J, Domen K. Highly dispersed niobium catalyst on carbon black by polymerized complex method as PEFC cathode catalyst. J Electrochem Soc 2009;156:B811–5. http://dx.doi.org/10.1149/1.3125801.

[18] Ohnishi R, Katayama M, Takanabe K, Kubota J, Domen K. Niobium-based catalysts prepared by reactive radio-frequency magnetron sputtering and arc plasma methods as non-noble metal cathode catalysts for polymer electrolyte fuel cells. Electrochim Acta 2010;55:5393–400. http://dx.doi.org/10.1016/j.electacta.2010.04.090.

[19] Nowak I, Ziolek M. Niobium compounds: preparation, characterization, and application in heterogeneous catalysis. Chem Rev 1999;99:3603–24.

[20] Wachs IE, Jehng J-M, Deo G, Hu H, Arora N. Redox properties of niobium oxide catalysts. Catal Today 1996;28:199–205. http://dx.doi.org/10.1016/0920-5861(95)00229-4.

[21] Fang B, Liu X, Wang X, Duan S. The mechanism of surface modification of a MCFC anode. J Electroanal Chem 1998;441:65–8. http://dx.doi.org/10.1016/S0022-0728(97)00202-7.

[22] Fang B, Chen H. A new candidate material for molten carbonate fuel cell cathodes. J Electroanal Chem 2001;501:128–31. http://dx.doi.org/10.1016/S0022-0728(01)00379-5.

[23] Ahonen M, Pessa M, Suntola T. A study of ZnTe films grown on glass substrates using an atomic layer evaporation method. Thin Solid Films 1980;65:301–7. http://dx.doi.org/10.1016/0040-6090(80)90240-0.

[24] Haukka S, Kytökivi A, Lakomaa E-L, Lehtovirta U, Lindblad M, Lujala V, et al. The utilization of saturated gas-solid reactions in the preparation of heterogeneous catalysts. In: Poncelet G, Martens J, Delmon B, Jacobs PA, Grange P, editors. Stud. Surf. Sci. Catal., vol. 91. Elsevier; 1995. p. 957–66. ISSN 0167-2991, ISBN 9780444820785, http://dx.doi.org/10.1016/S0167-2991(06)81839-2. (http://www.sciencedirect.com/science/article/pii/S0167299106818392).

[25] Kukli K, Ritala M, Leskelä M, Lappalainen R. Niobium oxide thin films grown by atomic layer epitaxy. Chem Vap Depos 1998;4:29–34.

[26] Moutiers G, Cassir M, Piolet C, Devynck J. Thermodynamic and voltammetric study of oxygen systems in molten Na_2CO_3-K_2CO_3 (56-44 mol.%) eutectic at 750°C. Electrochim Acta 1991;36:1063–71. http://dx.doi.org/10.1016/0013-4686(91)85316-Y.

[27] Pecharsky VK, Zavalij PY. Fundamentals of powder diffraction and structural characterization of materials. 2nd ed. Spring Street, New York, NY 10013, USA: Springer; 2009.

[28] Gomes MAB, Bulhões LO de S, Castro SC de, Damião AJ. The electrochromic process at Nb_2O_5 electrodes prepared by thermal oxidation of niobium. J Electrochem Soc 1990;137:3067–70. http://dx.doi.org/10.1149/1.2086161.

[29] McIntyre NS, Cook MG. X-ray photoelectron studies on some oxides and hydroxides of cobalt, nickel, and copper. Anal Chem 1975;47:2208–13. http://dx.doi.org/10.1021/ac60363a034.

[30] Matienzo J, Yin LI, Grim SO, Swartz WE. X-ray photoelectron spectroscopy of nickel compounds. Inorg Chem 1973;12:2762–9. http://dx.doi.org/10.1021/ic50130a005.

[31] Mansour AN, Melendres CA. Characterization of α-$Ni(OH)_2$ by XPS. Surf Sci Spectra 1994;3:255–62. http://dx.doi.org/10.1116/1.1247754.

[32] Venezia AM, Bertoncello R, Deganello G. X-ray photoelectron spectroscopy investigation of pumice-supported nickel catalysts. Surf Interface Anal 1995;23:239–47. http://dx.doi.org/10.1002/sia.740230408.

[33] Payne BP, Biesinger MC, McIntyre NS. The study of polycrystalline nickel metal oxidation by water vapour. J Electron Spectrosc Relat Phenom 2009;175:55–65. http://dx.doi.org/10.1016/j.elspec.2009.07.006.

[34] Biesinger MC, Payne BP, Grosvenor AP, Lau LWM, Gerson AR, Smart RSC. Resolving surface chemical states in XPS analysis of first row transition metals, oxides and hydroxides: Cr, Mn, Fe, Co and Ni. Appl Surf Sci 2011;257:2717–30. http://dx.doi.org/10.1016/j.apsusc.2010.10.051.

[35] Özer N, Chen D-G, Lampert CM. Preparation and properties of spin-coated Nb2O5 films by the sol-gel process for electrochromic applications. Thin Solid Films 1996;277:162–8. http://dx.doi.org/10.1016/0040-6090(95)08011-2.

[36] Rojas E, Delgado JJ, Guerrero-Pérez MO, Bañares MA. Performance of NiO and Ni–Nb–O active phases during the ethane ammoxidation into acetonitrile. Catal Sci Technol 2013;3:3173–82. http://dx.doi.org/10.1039/C3CY00415E.

[37] Malinowska B. Etude electrochimique du nickel en milieu carbonate fondu en vue de son application a la realisation de cathodes de piles a combustibles. Paris: Paris 6; 1996.

[38] Aufray M, Menuel S, Fort Y, Eschbach J, Rouxel D, Vincent B. New synthesis of nanosized niobium oxides and lithium niobate particles and their characterization by XPS analysis. J Nanosci Nanotechnol 2009;9:4780–5. http://dx.doi.org/10.1166/jnn.2009.1087.

[39] Kaufherr N, Eichorst DJ, Payne DA. X-ray photoelectron spectroscopy studies of alkoxide-derived lithium niobate. J Vac Sci Technol A 1996;14:299–305. http://dx.doi.org/10.1116/1.579892.
[40] Trifonov AS, Lubenchenko AV, Polkin VI, Pavolotsky AB, Ketov SV, Louzguine-Luzgin DV. Difference in charge transport properties of Ni-Nb thin films with native and artificial oxide. J Appl Phys 2015;117:125704. http://dx.doi.org/10.1063/1.4915935.
[41] Oku M, Tokuda H, Hirokawa K. Final states after Ni2p photoemission in the nickel—oxygen system. J Electron Spectrosc Relat Phenom 1991;53:201–11. http://dx.doi.org/10.1016/0368-2048(91)85039-V.
[42] Moses AW, Flores HGG, Kim J-G, Langell MA. Surface properties of $LiCoO_2$, $LiNiO_2$ and $LiNi_{1-x}Co_xO_2$. Appl Surf Sci 2007;253:4782–91. http://dx.doi.org/10.1016/j.apsusc.2006.10.044.
[43] Pawlak DA, Ito M, Oku M, Shimamura K, Fukuda T. Interpretation of XPS O (1s) in mixed oxides proved on mixed perovskite crystals. J Phys Chem B 2002;106:504–7. http://dx.doi.org/10.1021/jp012040a.
[44] Yazici MS, Selman JR. Dissolution of partially immersed nickel during in situ oxidation in molten carbonate: cyclic, stripping and square wave voltammetry measurements. J Electroanal Chem 1998;457:89–97. http://dx.doi.org/10.1016/S0022-0728(98)00126-0.
[45] Antolini E. Behaviour of Ni, NiO and $Li_xNi_{1-x}O$ in molten alkali carbonates. J Mater Sci 2000;35:1501–5. http://dx.doi.org/10.1023/A:1004745332382.
[46] Nishina T, Takizawa K, Uchida I. Electrochemical characterization of in situ NiO formation in a molten carbonate. J Electroanal Chem Interfacial Electrochem 1989;263:87–96. http://dx.doi.org/10.1016/0022-0728(89)80126-3.
[47] Belhomme C, Cassir M, Tessier C, Berthoumieux E. Lithium depth profile in NiO molten carbonate fuel cell cathode by nuclear microprobe. Electrochem Solid-State Lett 2000;3:216–9. http://dx.doi.org/10.1149/1.1391006.
[48] Escudero MJ, Ringuedé A, Cassir M, González-Ayuso T, Daza L. Porous nickel MCFC cathode coated by potentiostatically deposited cobalt oxide: III. Electrochemical behaviour in molten carbonate. J Power Sources 2007;171:261–7. http://dx.doi.org/10.1016/j.jpowsour.2007.06.013.